Applied Physics Letters

Experimentally tailoring acoustic topological edge states by selecting the boundary type

Cite as: Appl. Phys. Lett. **117**, 033503 (2020); https://doi.org/10.1063/5.0015499
Submitted: 28 May 2020 . Accepted: 08 July 2020 . Published Online: 22 July 2020

Jiao Wang, Nan Gao, Hongkuan Zhang, Xiaoming Zhou, Chaofeng Lü, and Weiqiu Chen

Applied Physics Letters ARTICLE scitation.org/journal/apl

Experimentally tailoring acoustic topological edge states by selecting the boundary type

Cite as: Appl. Phys. Lett. **117**, 033503 (2020); doi: 10.1063/5.0015499
Submitted: 28 May 2020 · Accepted: 8 July 2020 ·
Published Online: 22 July 2020

Jiao Wang,[1] Nan Gao,[1,2] Hongkuan Zhang,[3] Xiaoming Zhou,[3] Chaofeng Lü,[4,5,a)] and Weiqiu Chen[1,5,a)]

AFFILIATIONS

[1]Key Laboratory of Soft Machines and Smart Devices of Zhejiang Province and Department of Engineering Mechanics, Zhejiang University, Hangzhou 310027, People's Republic of China
[2]Department of Physics, Hong Kong University of Science and Technology, Kowloon 999077, Hong Kong, People's Republic of China
[3]Key Laboratory of Dynamics and Control of Flight Vehicle, Beijing Institute of Technology, Beijing 100081, People's Republic of China
[4]Department of Civil Engineering, Zhejiang University, Hangzhou 310058, People's Republic of China
[5]Soft Matter Research Center, Zhejiang University, Hangzhou 310027, People's Republic of China

[a)]**Authors to whom correspondence should be addressed:** lucf@zju.edu.cn and chenwq@zju.edu.cn. **Tel./Fax:** 86-571-87951866

ABSTRACT

With the valley Hall effect, acoustic waves at a frequency in a new bandgap in the frequency spectrum opened by breaking the spatial symmetry of a unit cell in a particular metamaterial may propagate at the boundaries of the structure (edge state) or at the interface between two topologically different structures (interface state). In a previous study, we have numerically found that, when the acoustic wave propagates along the boundary of a single structure, the selection of the boundary type plays a decisive role in tailoring the frequency range covered by the edge state. We here experimentally verified the tailoring function of the different types of boundaries. In particular, it was shown that the attenuation of acoustic waves changes remarkably with the boundary type, which is of great significance in tailoring the propagation path. The present experimental study, along with our previous simulation results, provides solid guidance for the design of topological acoustic devices with diverse wave propagation paths.

The concept of a topological insulator stems from condensed matter physics—it is internally insulating, but electrons can move along its boundary or interface. As already demonstrated in electronic systems, topologically protected edge states with scattering immunity and unidirectional propagation behavior can be produced by breaking the time-reversal symmetry of a topological insulator.

In recent years, the concept of topological insulators has been generalized and extended to phononic crystals (PCs) and acoustic metamaterials (MMs) in an effort to manipulate the wave propagation path in an unprecedented manner.[1–8] By breaking the time-reversal symmetry or certain spatial symmetry,[9–11] the edge state of topological phononic crystals with robust wave propagation immune to scattering at defects or sharp corners was observed. The fundamental principles for constructing topological insulators include the quantum Hall effect, the spin Hall effect, and the valley Hall effect.[12–15] The essential difference among the three mechanisms lies in the way to break the degeneracy. The quantum Hall effect is associated with time-reversal symmetry breaking,[16–19] while both the spin Hall effect and the valley Hall effect[20–27] correspond to the spatial symmetry breaking of MMs.

The topological MMs with the three different mechanisms can generate interface states with anti-scattering properties successfully.[28–34] The use of different mechanisms has enriched the design of wave propagation paths in topological MMs and achieved rich results. Khanikaev *et al.*[17] proposed to break the time-reversal symmetry by adding air flow to the unit cells in MMs. There are two different kinds of boundary states: one is confined at the boundary of a single structure and the other is located at the interface between two topologically different structures. We name the first type as the edge state and the second type as the interface state to distinguish them from each other. Recently, Zhang *et al.*[35] made use of magnetic fluid to break the spatial symmetry and designed a topological MM based on the valley Hall effect to tune the path of wave propagation. In their experiment, in addition to the interface state located at the interface of the composite structure, a certain edge state also appears at a specific boundary.

While most existing studies on topological MMs are centered on the interface states with anti-scattering properties, we have paid our attention to the edge states. Particularly, we have noted that the shape of a boundary of a topological two-dimensional MM may be selected or modified by cutting the boundary unit cells along a line parallel with but below that boundary. Thus, Wang *et al.*[36] considered a particular MM by changing the structural symmetry from C_{6v} to C_{3v} and identified a definite relationship between the existence of the edge state and the boundary type. The frequency range of the edge state can be regulated by the boundary, so that it can exist within the full or certain partial frequency range of the bandgap, or even no edge state exists at the boundary. Combined with the interface state, various regulation ways of the acoustic wave propagation path were realized, and a method of tailoring the propagation path was, thus, proposed by Wang *et al.*[36] It is noted that the decisive function of the boundary type was found only through simulation. Therefore, the main purpose of this Letter is to illustrate experimentally the decisive role of the boundary by considering two composite structures with different boundaries.

The overall composite structure designed and adopted in the experiment is shown in Fig. 1(a), which is composed of regularly arranged arrays of aluminum columns [Fig. 1(b)] embedded in air. Figure 1(c) shows the geometric description of the basic unit in the structure. The structure consists of about 500 aluminum columns with a total size of $70 \times 50 \times 1$ cm (length $\times$ width $\times$ thickness). In this scenario, the thickness of the aluminum column is appropriate for the wavelength under consideration.

The whole structure in Fig. 1(a) includes two topologically different parts, and the parameter r takes -0.1 on the left side and 0.1 on the right side, respectively. It should be noted that rotating the aluminum columns on the left side ($r = -0.1$) with 180° gives rise to the right part ($r = 0.1$). Therefore, only one kind of aluminum column needs to be prepared in our experiment, which makes the process easier. The upper and lower boundaries of the structure are replaceable. We used the loudspeaker to generate a point sound source with a frequency of 5700 Hz. The acoustic wave propagates from the bulk to the boundaries. We collected the acoustic pressure at the top and bottom boundaries via a microphone to illustrate the tailoring function of the boundary type. A cover plate was used to prevent the acoustic wave from propagating beyond the structure.

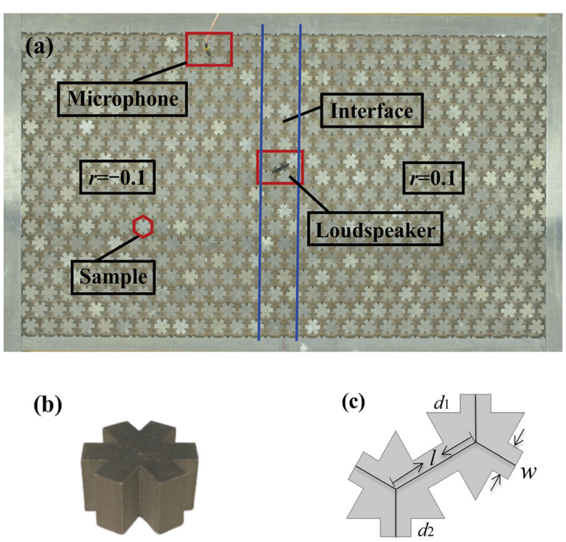

FIG. 1. (a) The composite structure designed and adopted in the experiment (the area sandwiched in two blue solid lines is the interface between the two topologically different parts); (b) the aluminum column; (c) the geometric parameters: $d_1 = c(1\text{-}r)/2$, $d_2 = c(1+r)/2$, and $c = 2\left(\sqrt{3}l - 2w\right)$, with r being a dimensionless parameter; and the lattice constant is $a = \sqrt{3}l$. $l = 1.5$ cm and $w = 0.5$ cm were adopted in this study.

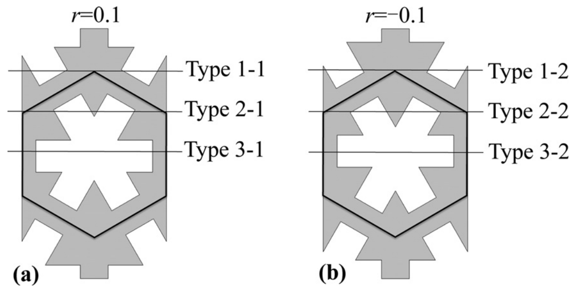

FIG. 2. (a) The four types of boundaries with $r = 0.1$; (b) the corresponding four boundaries at the same horizontal positions in the structure with $r = -0.1$.

Typical types of boundaries are shown in Fig. 2. Figure 2(a) exhibits the boundaries selected in the structure with $r = 0.1$. Type 1–1 is the case where a horizontal line passes through the center of the small triangle. The boundary of Type 3–1 is located at the middle position of the line connecting the centers of two adjacent triangles in the vertical direction. Figure 2(b) depicts the corresponding boundaries at the same horizontal positions in the structure with $r = -0.1$.

Figure 3 shows the unit cell, where the gray part represents air and the white part is the aluminum column with a thickness of 1 cm. This unit cell was adopted in the numerical simulation using the finite element calculation software COMSOL Multiphysics. The corresponding first Brillouin zone is shown in Fig. 3(b). When $r = 0$, the side lengths of the two adjacent triangles are equal, and the structure has the C_{6v} symmetry. That is, the rotation of the structure by 30° fully recovers its original configuration, and the structure holds the characteristic of mirror symmetry. However, when $r = 0.1$ or -0.1, the side lengths of the two adjacent triangles are no longer equal, and consequently, the lattice symmetry changes from C_{6v} to C_{3v}. At the same time, the mirror symmetry about the wave vector Γ–K is broken. In order to illustrate the change caused by a broken mirror symmetry, we plot the dispersion curves in Fig. 4.

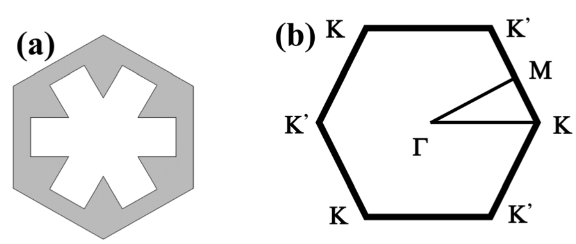

FIG. 3. (a) Schematics of a unit cell modeled using COMSOL Multiphysics; (b) the corresponding first Brillouin zone.

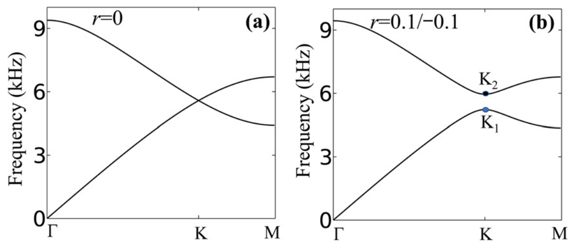

FIG. 4. The dispersion spectra: (a) $r = 0$; (b) $r = 0.1/-0.1$.

When $r \neq 0$, the symmetry of the structure is destroyed. Two topologically different structures are created in two opposite ways by taking $r = 0.1$ and $r = -0.1$, respectively. The dispersion curves shown in Fig. 4 indicate that there is a new bandgap induced by breaking the mirror symmetry about the wave vector Γ–K. When $r = 0$, the bandgap closes and degeneracy appears at the K point.

Figure 5 shows the acoustic valley pseudospin states at K_1 and K_2 points. The chirality of the valley pseudospin states is reversed from $r > 0$ to $r < 0$. This change is known as phase transition, which may be described mathematically by the valley Chern number ($\pm 1/2$). When the two structures with different topological properties are merged together, an interface state without backscattering will appear in the overlapping frequency range of the new bandgaps.

There are two kinds of topological states: one is located at the boundary of the single structure and the other is confined to the interface between two structures exhibiting different topological properties. We found in our previous study that the existence of the edge state depends on the boundary type.[36] We now consider four supercells with different types of boundaries (i.e., A, B, C, and D in Fig. 6), for which the dispersion spectra are shown in that figure.

In Fig. 6(a), supercells A and B have the same dispersion curves, with an isolated curve appearing in the bandgap, which represents the edge state. However, from the corresponding modes of Q_1 and Q_2

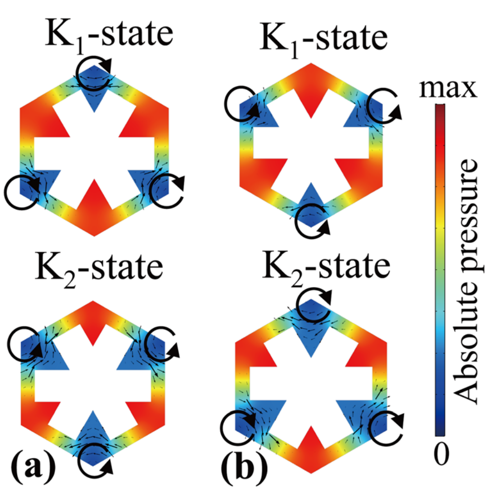

FIG. 5. The valley states at K_1 and K_2 for structures with (a) $r = 0.1$ and (b) $r = -0.1$, respectively.

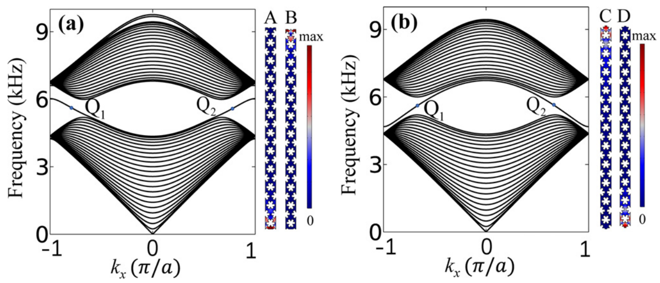

FIG. 6. Four types of supercells with different types of boundaries and the corresponding dispersion curves: (a) A, with $r = 0.1$, the top and bottom boundaries are type 1–1 and type 2–1, respectively; B, with $r = -0.1$, the top and bottom boundaries are type 1-2 and type 2-2, respectively; (b) C, with $r = 0.1$, the top and bottom boundaries both are type 3-1; D, with $r = -0.1$, the top and bottom boundaries both are type 3-2.

(both at 5700 Hz), it can be observed that the edge state of supercell A is at the bottom boundary, while the edge state of supercell B is located at the top boundary. Similarly, supercells C and D have the same dispersion spectrum, but the edge states appear at the opposite positions. The structure with $r = -0.1$ can be obtained by rotating 180° the structure with $r = 0.1$, and so the positions of the edge state are naturally exchanged. Supercells A and C have the same structural parameter $r = 0.1$, but the location of the edge state changes due to the different boundaries selected. A and B and C and D are superposed to build two structures with different boundaries.

The propagation path of the acoustic wave was first simulated in two structures composed of the regularly arranged supercells A and B and C and D. It should be noted that all the boundaries are taken to be sound hard in the simulation based on COMSOL Multiphysics. When the acoustic wave propagates in air, some of its energy will gradually dissipate with the increase in the distance away from the sound source. This energy dissipation due to air loss should be considered, and an imaginary part was, therefore, added to the velocity of the acoustic wave. In the simulation, the acoustic wave velocity and the loss factor were taken to be $c_{air} = 345$ m/s and $\eta = 0.018$, respectively.

The unique difference between the two structures is the types of top and bottom boundaries. As shown in Fig. 7, a point sound source with the frequency of 5700 Hz is loaded in the middle of the interface. The acoustic wave first propagates at the initial stage along the interface to the top and bottom edges. In structure I, the acoustic wave propagates at the second stage along the left side of the upper boundary and the right side of the lower boundary. However, in structure II, due to the different types of boundaries, the wave has selected a completely different propagation path at the second stage.

In the experiment, the acoustic pressures of the top two lines and the bottom two lines of the upper and lower boundaries were measured, respectively, to verify the tailoring function of the boundary. The counting way of the testing points is shown in Fig. 7(b). Take the first line at the bottom boundary as an example. Count from the left to the right, and collect the acoustic pressures at all 57 points on each line. The comparison of the measured acoustic pressure data and the simulation results is shown in Figs. 8 and 9. The ordinate represents the dimensionless sound pressure P/P_0, where P_0 is the pressure amplitude of the point source and P is the absolute pressure.

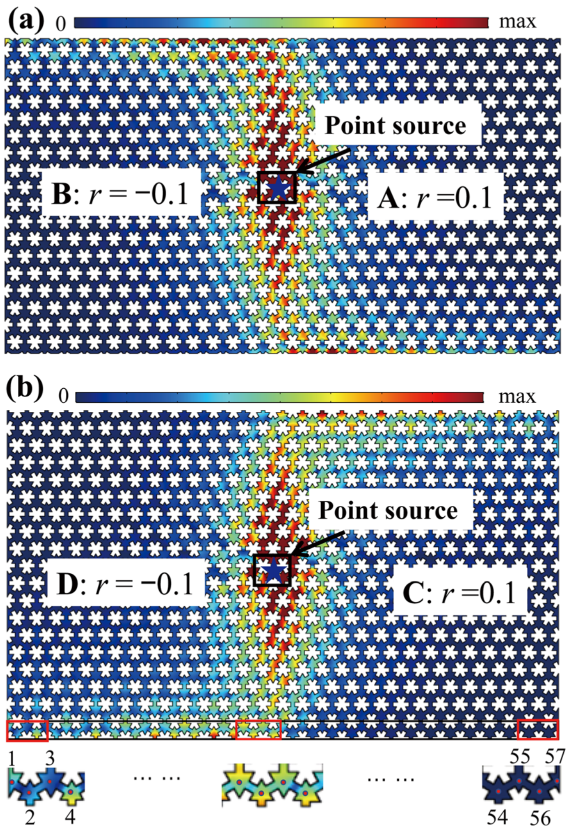

FIG. 7. Simulations of acoustic wave propagation: (a) structure I consisting of supercells A and B; (b) structure II consisting of supercells C and D.

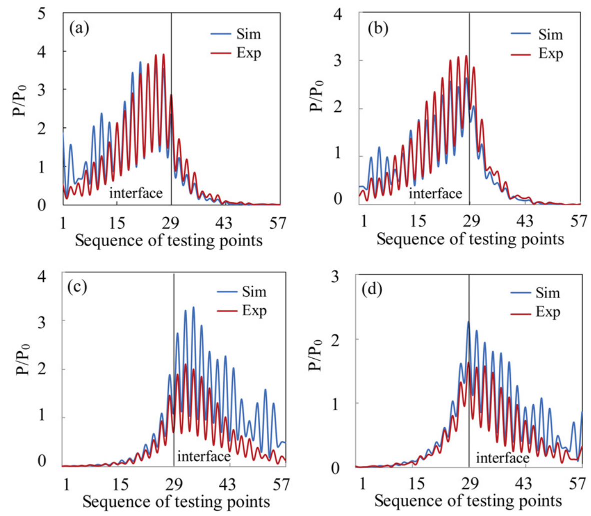

FIG. 8. Comparison between experiment and simulation for structure I.

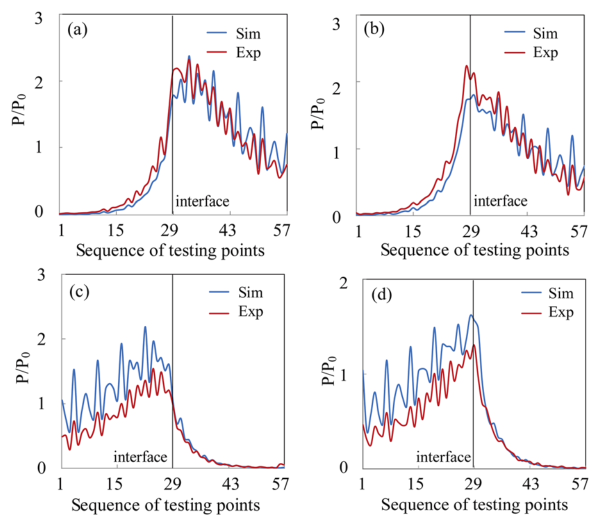

FIG. 9. Comparison between experiment and simulation for structure II.

As shown in Figs. 8 and 9, the experimental measurements match quite well with the numerical simulations. From Figs. 8(a) and 8(b), it can be seen that the acoustic pressure on the right side of the interface at the upper boundary decays exponentially and rapidly. This implies that the acoustic wave cannot propagate along the right-side boundary, that is, the wave frequency of 5700 Hz must be within the bandgap. In contrast, the left-side upper boundary decays in oscillation, which is attributed to the air damping. The left-side boundary supports the propagation of the acoustic wave. Similarly, the numerical results of structure II are in good agreement with the experimental data. Compared to structure I, the wave propagation path changes in an opposite way. This phenomenon is consistent with the analysis results of supercells A, B, C, and D as presented earlier. Through the comparison between experiment and simulation, it was verified that the selection of the boundary type can change the propagation path effectively.

In conclusion, tailoring the acoustic wave propagation path through selecting an appropriate boundary type was demonstrated experimentally. From the comparison, it was confirmed that the numerical findings in our previous study are reliable and also useful. In addition, it was uncovered that, both experimentally and numerically, the attenuation of acoustic waves depends greatly on the boundary type, and this property can be used to modify the propagation path effectively. It is also interesting that the frequency range wherein the edge state exists can be tuned, and so we may realize the wave filtering function through the selection of appropriate boundaries. This boundary filtering function can be easily verified numerically, but needs to be confirmed experimentally in a further study.

This work was supported by the National Natural Science Foundation of China (Nos. 11532001, 11621062, 11872329, and 11925206). Partial support from the Fundamental Research Funds for the Central Universities (No. 2016XZZX001-05) and the Shenzhen Scientific and Technological Fund for R & D (No. JCYJ20170816172316775) is also acknowledged.

DATA AVAILABILITY

The data that support the findings of this study are available from the corresponding author upon reasonable request.

REFERENCES

[1] P. Wang, Y. Zheng, M. C. Fernandes, Y. Sun, K. Xu, S. Sun, S. H. Kang, V. Tournat, and K. Bertoldi, "Harnessing geometric frustration to form band gaps in acoustic channel lattices," Phys. Rev. Lett. **118**, 084302 (2017).

[2] M. Xiao, G. Ma, Z. Yang, P. Sheng, Z. Q. Zhang, and C. T. Chan, "Geometric phase and band inversion in periodic acoustic systems," Nat. Phys. **11**, 240 (2015).

[3] F. Liu, X. Huang, and C. T. Chan, "Dirac cones at $k \rightarrow 0$ in acoustic crystals and zero refractive index acoustic materials," Appl. Phys. Lett. **100**, 071911 (2012).

[4] J. Yin, M. Ruzzene, J. Wen, D. Yu, L. Cai, and L. Yue, "Band transition and topological interface modes in 1D elastic phononic crystals," Sci. Rep. **8**, 6806 (2018).

[5] D. Torrent and J. Sánchez-Dehesa, "Acoustic analogue of graphene: Observation of Dirac cones in acoustic surface waves," Phys. Rev. Lett. **108**, 174301 (2012).

[6] M. P. Makwana, N. Laforge, R. V. Craster, G. Dupont, S. Guenneau, V. Laude, and M. Kadic, "Experimental observations of topologically guided water waves within non-hexagonal structures," Appl. Phys. Lett. **116**, 131603 (2020).

[7] C. He, S. Y. Yu, H. Wang, H. Ge, J. Ruan, H. Zhang, M. H. Lu, and Y. F. Chen, "Hybrid acoustic topological insulator in three dimensions," Phys. Rev. Lett. **123**, 195503 (2019).

[8] Y. Wang, Y. Wang, B. Wu, W. Chen, and Y. Wang, "Tunable and active phononic crystals and metamaterials," Appl. Mech. Rev. **72**, 040801 (2020).

[9] B. Z. Xia, S. J. Zheng, T. T. Liu, J. R. Jiao, N. Chen, H. Q. Dai, D. J. Yu, and J. Liu, "Observation of valley like edge states of sound at a momentum away from the high-symmetry points," Phys. Rev. B. **97**, 155124 (2018).

[10] J. Mei, Y. Wu, C. T. Chan, and Z. Q. Zhang, "First-principles study of Dirac and Dirac-like cones in phononic and photonic crystals," Phys. Rev. B **86**, 035141 (2012).

[11] S. Li, D. Zhao, H. Niu, X. Zhu, and J. Zang, "Observation of elastic topological states in soft materials," Nat. Commun. **9**, 1370 (2018).

[12] Y. Chen, X. Liu, and G. Hu, "Topological phase transition in mechanical honeycomb lattice," J. Mech. Phys. Solids **122**, 54 (2019).

[13] T. W. Liu and F. Semperlotti, "Experimental evidence of robust acoustic valley Hall edge states in a nonresonant topological elastic waveguide," Phys. Rev. Appl. **11**, 014040 (2019).

[14] B. H. Nguyen, X. Zhuang, H. S. Park, and T. Rabczuk, "Tunable topological bandgaps and frequencies in a pre-stressed soft phononic crystal," J. Appl. Phys. **125**, 095106 (2019).

[15] Z. Zhang, Y. Tian, Y. Cheng, Q. Wei, X. Liu, and J. Christensen, "Topological acoustic delay line," Phys. Rev. Appl. **9**, 34032 (2018).

[16] Z. G. Chen and Y. Wu, "Tunable topological phononic crystals," Phys. Rev. Appl. **5**, 054021 (2016).

[17] A. B. Khanikaev, R. Fleury, S. H. Mousavi, and A. Alù, "Topologically robust sound propagation in an angular-momentum-biased graphene-like resonator lattice," Nat. Commun. **6**, 8260 (2015).

[18] P. Wang, L. Lu, and K. Bertoldi, "Topological phononic crystals with one-way elastic edge waves," Phys. Rev. Lett. **115**, 104302 (2015).

[19] Z. Yang, F. Gao, X. Shi, X. Lin, Z. Gao, Y. Chong, and B. Zhang, "Topological acoustics," Phys. Rev. Lett. **114**, 114301 (2015).

[20] J. Lu, C. Qiu, L. Ye, X. Fan, M. Ke, F. Zhang, and Z. Liu, "Observation of topological valley transport of sound in sonic crystals," Nat. Phys. **13**, 369 (2017).

[21] C. Qiu, M. Ke, H. He, Z. Liu, X. Wen, and J. Lu, "Acoustic Dirac degeneracy and topological phase transitions realized by rotating scatterers," J. Appl. Phys. **123**, 091703 (2018).

[22] J. Vila, R. K. Pal, and M. Ruzzene, "Observation of topological valley modes in an elastic hexagonal lattice," Phys. Rev. B **96**, 134307 (2017).

[23] L. Ye, C. Qiu, J. Lu, X. Wen, Y. Shen, M. Ke, F. Zhang, and Z. Liu, "Observation of acoustic valley vortex states and valley-chirality locked beam splitting," Phys. Rev. B **95**, 174106 (2017).

[24] H. Dai, T. Liu, J. Jiao, B. Xia, and D. Yu, "Double Dirac cone in two-dimensional phononic crystals beyond circular cells," J. Appl. Phys. **121**, 135105 (2017).

[25] Y. Guo, T. Dekorsy, and M. Hettich, "Topological guiding of elastic waves in phononic metamaterials based on 2D pentamode structures," Sci. Rep. **7**, 18043 (2017).

[26] C. He, X. Ni, H. Ge, X. C. Sun, Y. Bin Chen, M. H. Lu, X. P. Liu, and Y. F. Chen, "Acoustic topological insulator and robust one-way sound transport," Nat. Phys. **12**, 1124 (2016).

[27] S. H. Mousavi, A. B. Khanikaev, and Z. Wang, "Topologically protected elastic waves in phononic metamaterials," Nat. Commun. **6**, 8682 (2015).

[28] J. Lu, C. Qiu, S. Xu, Y. Ye, M. Ke, and Z. Liu, "Dirac cones in two-dimensional artificial crystals for classical waves," Phys. Rev. B **89**, 134302 (2014).

[29] J. Lu, C. Qiu, M. Ke, and Z. Liu, "Valley vortex states in sonic crystals," Phys. Rev. Lett. **116**, 093901 (2016).

[30] T. W. Liu and F. Semperlotti, "Tunable acoustic valley-Hall edge states in reconfigurable phononic elastic waveguides," Phys. Rev. Appl. **9**, 14001 (2018).

[31] T. Kariyado and Y. Hatsugai, "Manipulation of Dirac cones in mechanical graphene," Sci. Rep. **5**, 18107 (2015).

[32] B. Xia, G. Wang, and S. Zheng, "Robust edge states of planar phononic crystals beyond high-symmetry points of Brillouin zones," J. Mech. Phys. Solids **124**, 471 (2019).

[33] W. Zhou, Y. Su, Muhammad, W. Chen, and C. W. Lim, "Voltage-controlled quantum valley Hall effect in dielectric membrane-type acoustic metamaterials," Int. J. Mech. Sci. **172**, 105368 (2020).

[34] Z. Tian, C. Shen, J. Li, E. Reit, H. Bachman, J. E. S. Socolar, S. A. Cummer, and T. Jun Huang, "Dispersion tuning and route reconfiguration of acoustic waves in valley topological phononic crystals," Nat. Commun. **11**, 762 (2020).

[35] Q. Zhang, Y. Chen, K. Zhang, and G. Hu, "Programmable elastic valley Hall insulator with tunable interface propagation routes," Extreme Mech. Lett. **28**, 76 (2019).

[36] J. Wang, Y. Huang, and W. Chen, "Tailoring edge and interface states in topological metastructures exhibiting the acoustic valley Hall effect," Sci. China: Phys., Mech. Astron. **63**, 224611 (2020).